A 10 μm pitch, SXGA Multifunctional IRFPA ROIC with In-Pixel Laser Event Detection and High Dynamic Range Imaging

C.G. Jakobson, I. Pivnik, R. Dobromislin, G. Zohar, O. Cohen, Y. Chaham, N. Shiloah, R. Talmor, E. Ilan, I. Nevo, W. Freiman, N. Ben Ari, R. Fruhi, T. Shapira, R. Fraenkel

SCD Semiconductor Devices – P.O. Box 2250, Haifa, 31021, Israel
**Corresponding author: claudio@scd.co.il*

***Abstract*— Modern infrared focal plane arrays require many in-pixel multimode capabilities. One purpose is to include variable gain that enables imaging in wide dynamic range scenarios. A second purpose is to include special in pixel functions that can provide event detection and analysis at the pixel level. This work presents a new readout integrated circuit that provides imaging together with laser pulse detection. The standard imaging modes at low and medium gain are based on direct injection, a low noise imaging mode with high gain based on charge transimpedance amplification is also implemented. A special laser feature analyzes in real time the AC component of the signal integration to recognize the presence of a laser event and combines the image with asynchronous or synchronous laser detection. The image pixel size is 10x10 μm^2 providing an image resolution of 1280x1024 that is combined with laser detection based on binning of four pixels with a resolution of 640x512. At low noise imaging the full well capacity is 12ke$^-$, and goes up to 0.5Me$^-$ and 1Me$^-$ for medium and low gain imaging, respectively. The minimum laser pulse detectability is 500e$^-$.**

Keywords: ROIC, Multifunctional, SWIR, Laser Pulse Detection, Infrared Detector, InGaAs, Low Light Level

I. INTRODUCTION

Many systems require the integration of Infrared Focal Plane Arrays (IRFPAs) with multifunction capabilities in order to combine imaging with laser-based active modes and laser detection. The multifunctional Read-Out Integrated Circuit (ROIC) presented in this work combines Standard Imaging (SIM), Low Noise Imaging (LNIM), Region of Interest (ROI) selection, Active Imaging (AI), and Laser Pulse Detection (LPD). The LPD feature can be synchronous (SLPD) or asynchronous (ALPD).

In order to provide the LPD capabilities the ROIC includes an in-pixel AC laser event detection based on our patented pixel architecture [1]. This circuit enables two-dimensional highly sensitive laser detection that is performed simultaneously with imaging acquisition. In all cases the fast AC signal is too small to be detected at the integrated image even by precise differentiation of consecutive frames and dedicated image signal processing. In previous work we have shown a 640x512 multifunctional ROIC including laser detection features [2-3]. This work presents a new ROIC that integrates similar multifunctional capabilities and laser detection with a higher resolution image 1280x1024 (SXGA) reducing the pixel pitch to 10 μm. The CMOS ROIC is flip-chip bonded to an InGaAs IRFPA [4] and provides a digital output signal. The multifunctional ROIC achieves a combined 89 dB Dynamic range at a maximum frame rate of 160 Frames per Second (FPS). AI is possible by reducing the ROIC integration time constant at a specific ROI. In AI mode the integration time can be reduced to 1μs with an integration time constant below this value. In other modes the integration is controllable between 100μs and 100ms. The laser detectability goes down to 500 electrons.

II. ROIC ARCHITECTURE

Fig.1 shows the novel multifunctional ROIC pixel architecture indicating the single and shared pixel elements. Sharing is done in order to enable the integration of all the pixel functions in a 10 μm pitch. The circuits placed at the shared region are those corresponding to the laser detection and part of the column readout. The ROIC digital output is converted by 13 bit column-parallel ADCs [5-6] with a dynamic range of 74 dB consuming 40 μW per channel. SLPD and ALPD are provided by a separate single bit that is added as the 14th bit to the output word.

At SIM the ROIC operates the detectors in injection mode and integrates its photocurrent as it is generally done in IR imaging [7]. The pixel image can be integrated either by Direct Injection (DI) or Capacitive Trans-Impedance Amplification (CTIA). Using DI the ROIC can be configured to provide two different SIM gains, at low gain the full well capacity is 1Me$^-$ and at medium gain it is 0.5Me$^-$. Using the CTIA circuits the ROIC provides LNIM with a full well capacity of 12ke$^-$. Integration While Read (IWR) is possible at the SIM modes. The imaging shutter is global as usually required in IRFPA applications.

A Band-Pass Filter (BPF) is shown in Fig. 1 that enables the LPD functions by providing a signal that is

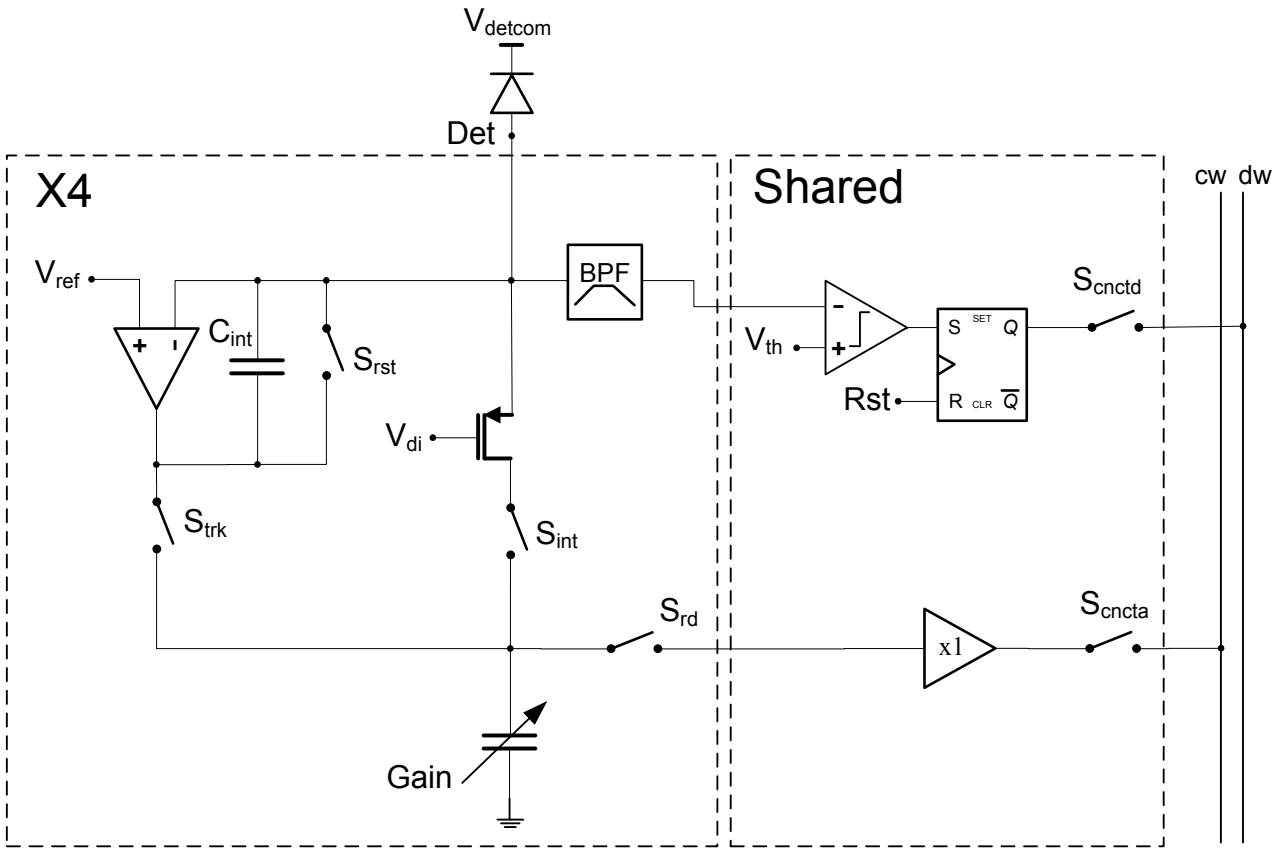

Fig. 1. Multifunctional pixel architecture

related to the AC variations at the detector. The output of the BPF is shared and compared to a threshold voltage V_{th} by a comparator implemented at the shared pixel area. The output of the comparator is latched and read at the digital wire (dw) together with the buffered pixel output that is read through the column wire (cw). A positive bit at dw indicates that a laser event occurred during the integration.

Fig. 2 shows a microphotograph of the ROIC die. In order to reduce the frame read time two ADC rows are implemented at the upper and bottom sides of the pixel matrix. The digital controller is placed at the left side of the die and controls the integration timing, the frame read timing and other signals required by the configuration mode.

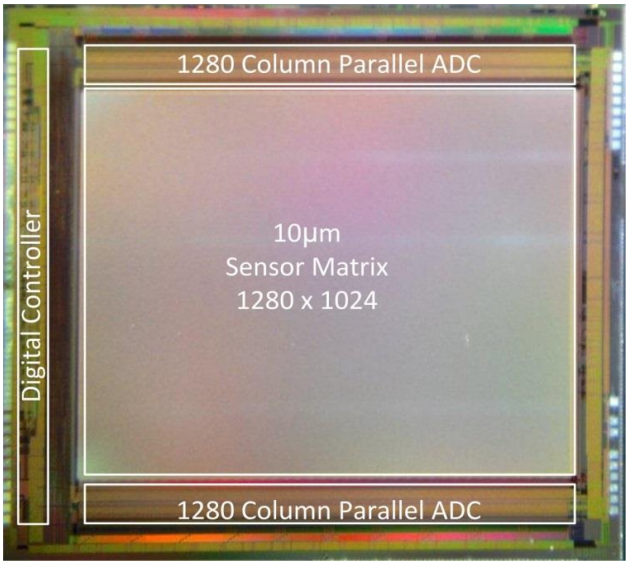

Fig. 2. Die microphotograph

III. Simulations and Measurements

Fig. 3 shows a Short Wave Infrared (SWIR) image

Fig. 3. SWIR Image from an InGaAs sensor with simultaneous laser detection, the laser spot is reflected at the license number of the parked car

from an InGaAs sensor array combined with ALPD. The low power NIR laser is pointed at the license plate of a car at our parking lot. Laser reflections are present at the plate triggering the LPD circuitry, the image indicates the LPD bit in red, some rounding of the laser detection is observed at Fig. 3, this is due to optic effects.

Fig. 4 shows the measured dark temporal noise at LNIM and SIM modes using an InGaAs IRFPA. The average noise at LNIM is 35e$^-$ and at medium gain SIM it is 210 e$^-$. The measured full-well capacity at these modes is 12ke$^-$ at LNIM, 0.5M e$^-$ at medium gain SIM, and 1Me$^-$ at low gain SIM.

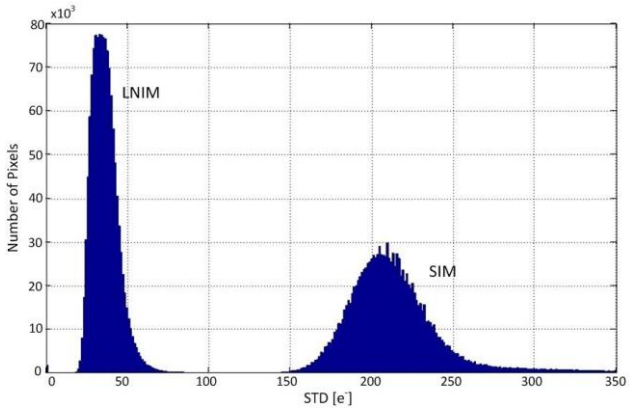

Fig. 4. Readout noise histogram: LNIM and SIM modes of operation

Fig. 5 shows the simulated and the measured laser detectability and False Alarm Rate (FAR) at dark as function of the threshold voltage for laser pulses of 500e$^-$, 750e$^-$ and 1000e$^-$. The measured values are indicated by symbols while the simulated values are shown by dashed lines. The simulation includes the MonteCarlo variations of the ROIC due to process as well as the detection circuit noise. The figure shows that simulated and measured values are in good agreement. At 500 e$^-$ the laser detection probability (the difference between detection and FAR percentages) is up to 70%. The measurements have been done with 30msec integration time.

To emphasize the LPD capabilities of the ROIC we compare the laser detection by the in-pixel circuit to a bared-eye image of the detected laser spot in a medium gain SIM scale. Fig. 6 shows the series of SIM captured images. The laser spot is pointed at the center of a smooth background with low illumination level and its corresponding charge is indicated in each image. Even in this friendly conditions the laser starts to be visible only at 10000 e$^-$. Comparing to values at Fig. 5 this is about 20 times the sensitivity limit of the the ROIC LPD.

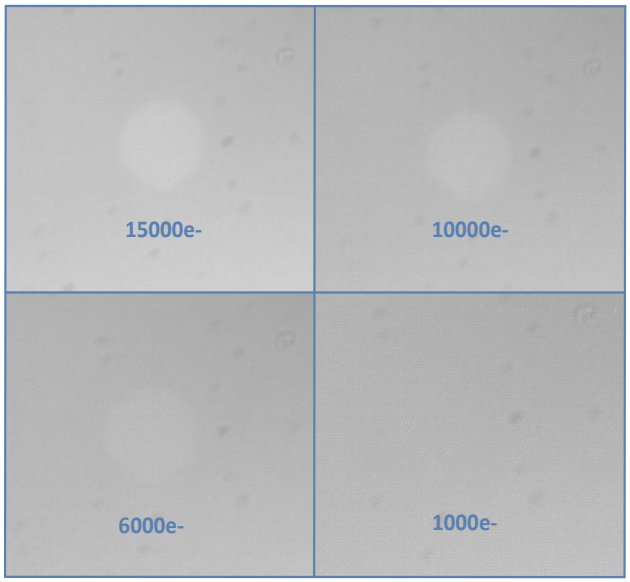

Fig. 6. Visibility of the detected laser spot by the bared-eye in images captured at medium gain SIM mode.

The Residual Non-Uniformity (RNU) of the ROIC and the InGaAs IRFPA after two-point Non-Uniformity Correction (NUC) is shown in Fig. 7. The graphs correspond to two different imagers. The isolated point correspond to the measured RNU for different well fill separated by steps of approximately 10%, an arbitrary polynomial fit is shown by the dashed line. The RNU

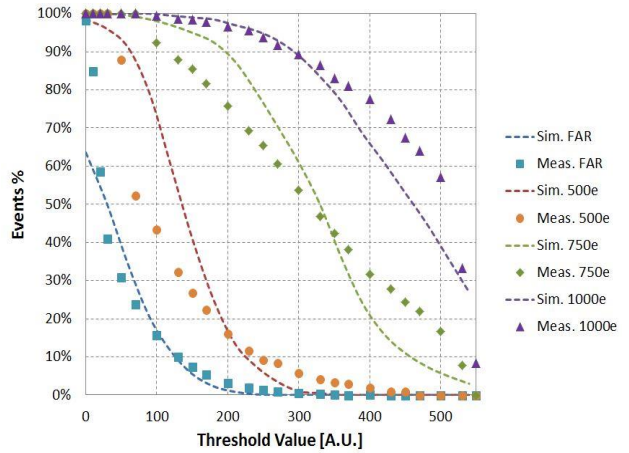

Fig. 5. Percentage of FAR and detection events for several laser pulses corresponding to 500e$^-$, 750 e$^-$, and 1000e$^-$. The individual marks indicate measured values and the dashed lines indicate simulated values.

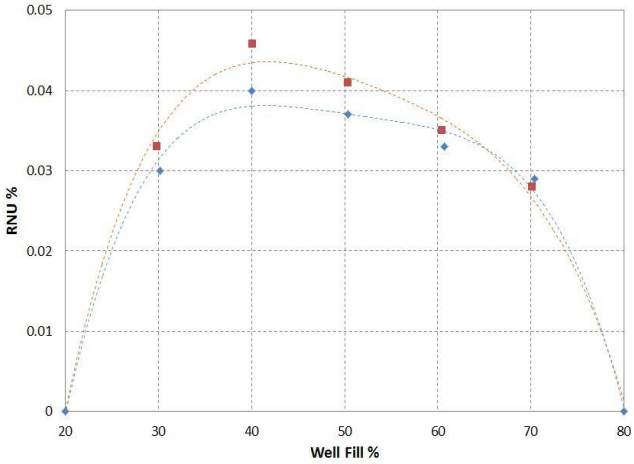

Fig. 7. RNU of the InGaAs IRFPA and ROIC as a function of the well fill. The RNU is calculated after two-point NUC.

values are below 0.05%.

Fig. 8 shows the non-linearity of the IRFPA and ROIC of Fig. 7 measured with variable irradiance and integration time of 10msec. The values are shown up to 40% well fill and the corresponding non-linearity is approximately 0.05% of the dynamic range. In a 100% full scale well fill the non-linearity is below 0.1% of the dynamic range. As in the previous figure the symbols indicate measured values while the dashed line is an arbitrary polynomial fit.

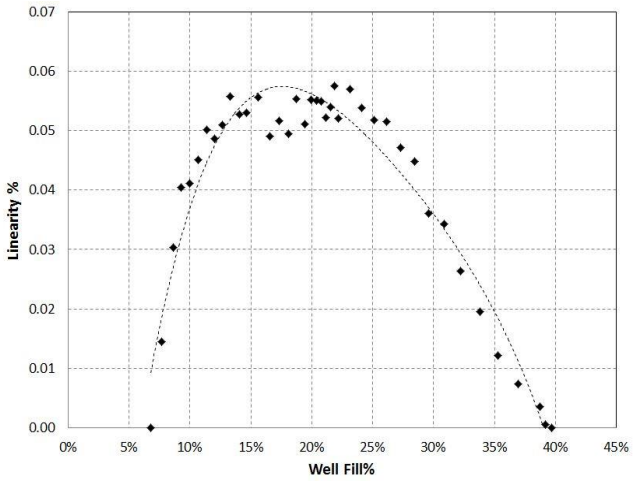

Fig. 8. ROIC and InGaAs IRFPA linearity vs. well fill for variable irradiance and integration time of 10ms.

As previously mentioned, another special laser-based function of the ROIC is the AI mode. For this mode fast ROIC integration time constant is designed. The reduction of the time constant has been determined by simulations and is controlled over a specific and selectable ROI. Depending on the ROI the time constant for AI can be reduced to values below 1µs.

IV. SUMMARY

We have presented a multifunctional ROIC, and its performance when integrated with an InGaAs IRFPA. The ROIC integrates imaging signals at LNIM mode with full well capacity of 12ke$^-$, and at SIM mode with full well capacity of 0.5Me$^-$ and 1Me$^-$.

Imaging can be integrated over a selectable ROI and with fast AI. The integration is controlled by a global shutter and the integrated signal can be read during the integration time at the IWR mode.

Besides imaging capabilities the ROIC is able to detect the presence of a laser pulse during the image integration by isolating the AC component of the event signal. The detection can be made synchronously to the laser pulse or asynchronously with a sensitivity of 500 e$^-$.

Table 1 summarizes the main imager performance parameters.

TABLE I
ROIC MAIN PERFORMANCE

PARAMETER		VALUE
Resolution	Imaging	1280x1024
	Laser detection	640x512
Well Capacity	LNIM	12ke-
	SIM medium gain IWR	0.5Me-
	SIM low gain ITR	1M e-
Readout Noise	LNIM	35e-
	SIM medium gain	210e-
	SIM low gain	350 e-
Power dissipation at 60FPS		<150mW
Laser detection sensitivity		500 e-
Combined dynamic range		89dB
Maximum frame rate		160Hz
Minimum selectable ROI		32 x 32
Minimum active imaging time constant		<1µs
SIM Residual Non Uniformity		<0.05% of DR
ROIC Non Linearity		<0.1% of DR

V. ACKNOWLEDGMENTS

The work presented here was supported over the years by the Chief Scientist of the Israeli Ministry of Economics. We are in debt to a large group of engineers and technicians who conducted this work. Their dedicated work and contribution to the development and production of the detectors is highly appreciated.

VI. REFERENCES

[1] S. Elkind, E. Ilan, R. Dobromislin, "Detector pixel signal readout circuit using an AC signal component in implementing an event detection mode per pixel", US Patent US9215386 B2, 2015.

[2] L. Langof et al. "Advanced multi-function infrared detector with on-chip processing", Proc. of SPIE 8012, Infrared Tech. and Applicat. XXXVII, 80120F, 2011.

[3] L. Shkedy et al. "Multifunction InGaAs detector with on-chip signal processing", Proc. of SPIE Vol. 8704 87042I-1, 2013.

[4] R. Fraenkel et al., "High definition 10µm pitch InGaAs detector with asynchronous laser pulse detection mode", Infrared Technology and Applications XLII, 981903, 2016.

[5] O.Nesher et al. " High resolution 1280x1024 15µm pitch compact InSb IR detector with on-chip ADC", Proc. SPIE IR Tech. & App. XXXV, vol. 7298, pp. 1-9. 2009.

[6] M.F. Snoeij, A.J.P. Theuwissen, K.A.A.Makinwa, J.H. Huising, "Multiple-ramp column parallel ADC architectures for CMOS image Sensors", IEEE J. of Solid State Circuits, vol. 42, no. 12, pp. 2968-77, Dec. 2007.

[7] A. Rogalski, "Infrared detectors: an overview", Infrared Physics & Technology 43 pp. 187–210, 2002.